

Solar Photocatalysis of TiO₂ Supported Natural Palygorskite Nanofibers Elaborated by a One_Pot Mechanochemical Route

Lakbita Omar¹, Rhouta Benaissa^{2*}, Goetz Vincent³, Maury Francis⁴, Plantard Gaël³, Daoudi Lahcen⁵

¹Mohammed VI Polytechnic University (UM6P), Marrakech, Morocco

²IMED_Lab, Faculty of Sciences and Technologies, Cadi Ayyad University, Marrakech, Morocco

³PROcédés Matériaux et Energie Solaire, Rambla de la Thermodynamique, PROMES_CNRS, UPR 8521, Perpignan, France

⁴CIRIMAT, Université de Toulouse, Toulouse, France

⁵Laboratoire de Geoscience et Géoenvironnement, Faculté des Sciences et Techniques Guéliz, Université Cadi Ayyad, Marrakech Morocco

Email: *plantard@univ-perp.fr

How to cite this paper: Omar, L., Benaissa, R., Vincent, G., Francis, M., Gaël, P. and Lahcen, D. (2022) Solar Photocatalysis of TiO₂ Supported Natural Palygorskite Nanofibers Elaborated by a One_Pot Mechanochemical Route. *Journal of Minerals and Materials Characterization and Engineering*, 10, 254-274.

<https://doi.org/10.4236/jmmce.2022.103020>

Received: March 30, 2022

Accepted: May 23, 2022

Published: May 26, 2022

Copyright © 2022 by author(s) and Scientific Research Publishing Inc. This work is licensed under the Creative Commons Attribution International License (CC BY 4.0).

<http://creativecommons.org/licenses/by/4.0/>



Open Access

Abstract

This study reports the successful synthesis of supported TiO₂-Palygorskite nanocomposites by a one-pot dry mechanochemical route. Indeed, the elaboration procedure involved an in-situ reaction between accessories carbonates present in raw fibrous palygorskite clay and titanyl sulfate (TiOSO₄) precursor under variable grinding conditions, essentially ball/solid matter mass ratio and rotation velocity. This yielded after air annealing at 600°C for 1 h to the immobilization of anatase TiO₂ nanoparticles (≈8 nm of average size) as evidenced by XRD and TEM analyses. Once the conditions of elaboration were optimized, the photocatalytic properties were evaluated under 3 conditions: artificial UV radiation, artificial solar radiation (UV + visible range) and under dynamic solar illumination taking into account the discontinuities of the solar resource. The results allowed the estimation and comparison of the catalyst's capabilities and showed its ability to work under natural irradiation. The so developed supported photocatalysts TiO₂/Palygorskite exhibited a good activity towards the removal of Orange G (OG) dye from aqueous media under artificial UV and natural solar radiations.

Keywords

TiO₂, Palygorskite, Mechanochemical Synthesis, Nanocomposite, Solar Photocatalysis, Wastewater Treatment

1. Introduction

Heterogeneous photocatalytic oxidation recently has emerged as an efficient alternative process for wastewater treatment [1]-[6]. The principle of this technique relies on the creation of reactive species as holes (h^+) and hydroxyl radicals (OH^\bullet) upon irradiating a semiconductor oxide with an energy source ($h\nu$) higher than its energy band gap [1] [6]. In optimized processes, the highly oxidizing species so generated are able to induce complete mineralization of organic pollutants into CO_2 and H_2O [1]. TiO_2 anatase is the most active semiconductor oxide in photocatalysis and is besides widely used owing to its numerous advantages, for instance, non-harmfulness, low cost, and chemical inertness [1]. Several wet methods, including sol-gel [7] [8] [9], flame aerosol [10], solvothermal [11] were reported for the synthesis of TiO_2 powder. Interestingly, a dry method based on grinding powders of carbonate compound, namely Na_2CO_3 and a Ti molecular precursor such as titanium sulfide (TiS_2) [12] [13] and titanyl sulfate ($TiOSO_4 \cdot 2H_2O$) [14] [15] [16] was also reported to synthesize pure TiO_2 powder. However, the direct use of TiO_2 in the form of nano-powder (*e.g.*, commercial Degussa P25 powder [10]) raises several problems such as agglomeration of the nanoparticles during the process, which reduces photocatalytic efficiency [17]. Additionally, recovering of micron sized aggregated particles from water decontaminated by TiO_2 slurry needs to implement costly microfiltration processes [2] [6] [17] [18]. To overcome these drawbacks, researches focused on improving photocatalytic processes by the development of TiO_2 supported photocatalysts, in particular starting with natural highly dispersed materials as support.

The solar resource is a sustainable energy by definition and available for many applications. For photo-oxidation applications, capacities are limited because most catalysts are only sensitive to ultra violet (UV) radiation in the spectrum. This represents only 5% of the solar radiation, resulting in limited performance for solar installations. A second characteristic of the solar resource is its intermittent nature, which is due to the daily (day/night) and seasonal cycle, but also to meteorological effects such as the passage of clouds or heavy cloud cover. Thus, to meet these constraints, the catalysts developed must have photocatalytic properties that allow the use of the solar resource and manage the fluctuations linked to this resource. This implies catalysts with both photo-excitation characteristics to produce radicals and sorption characteristics to store the molecules during low sunlight phases.

Among the support materials envisaged, clay minerals are considered promising owing to their interesting inherent multi-functional properties such as their adsorption capacity, high surface area, multiscale porosity, and ability to be grafted by chemical compounds [18]-[25]. In this respect, some authors more recently reported $CeO_2_WO_3_Palygorskite/TiO_2$ catalysts elaborated by impregnation method [26] and TiO_2 supported on three natural clays with different morphologies carried out by sol-gel route [27]. In the same way, we reported some years ago the immobilization of TiO_2 anatase nanoparticles (NPs) with an

average size of 10 nm onto particles surfaces of beidellite [28] and nanofibers surfaces of palygorskite [29] via a colloidal sol-gel route. Beidellite and palygorskite were both natural clay minerals sampled in Morocco from Agadir basin and Marrakech High Atlas regions, respectively. They were purified, characterized, and specifically functionalized to be used as catalytic supports in the wet synthesis methods employed [28] [29]. Photocatalytic tests performed in presence of these TiO₂ supported clay nanocomposites towards the degradation of Orange G dye (OG) were promising in that they interestingly exhibited a photoactivity normalized to the TiO₂ amount higher than that of pure TiO₂ micropowder commercially available as Degussa P25.

Nevertheless, the synthesis of these supported photocatalysts is generally achieved via colloidal [21] [27] or solvothermal [30] or pillaring [20] wet routes, which on one hand required previous purifying and/or homoionisation with Na⁺ ions of clay minerals. On the other hand, these elaboration methods involved several steps so that they are laborious, time and solvents consuming and yielding to small laboratory amounts. Thereby, they have a low capacity to be transferred to industrial scale. Thus, there is a need to find out alternative synthesis method to overcome these wet routes issues.

The aim of this work is to show the potential of these materials for a solar photo-oxidation application. It is divided into three parts. The first part aims at elaborating TiO₂ supported palygorskite by a free-solvent one-pot mechanochemical method starting from powders of raw palygorskite (Pal) clay and titanil sulfate (TiOSO₄·2H₂O) precursor. This dry synthesis route was smartly based on *in-situ* reaction between carbonates accessorially available in raw clay and a Ti molecular precursor to immobilize resulting TiO₂ particles on the surface of palygorskite fibers or in the vicinity of their surface in the tangle of fibers. Synthesis conditions were optimized by studying the influence of the composition ratio palygorskite clay/TiOSO₄·2H₂O and grinding velocity. The second step is to select the optimal conditions for the development of a material in order to control the photocatalytic properties. The so elaborated TiO₂-Pal nanocomposites were afterwards characterized at a multi-scale level using *in situ* X-ray diffraction (XRD (X'pert powders Philips diffractometer)), Scanning Electron Microscopy (SEM (SEM-FEG, Hitachi S-4500)) and Transmission Electron Microscopy (TEM (JEOL JEM 2010)). The originality lies in a global approach starting from the elaboration of the catalysts, their optimization to test their photocatalytic potential. The aim being to evaluate the photo-oxidation capacities under solar conditions, our step-by-step approach involves three stages. Measurements are carried out under controlled irradiation conditions, both in terms of spectral distribution and flux density (artificial UV and solar irradiation) with the aim of modelling the photo-oxidative capacities of the catalysts. Finally, the photo-oxidation capacities are measured and modelled under natural irradiation, taking into account the characteristics of solar radiation: spectral distribution and flux density discontinuities. Thus, photo-activities were evaluated towards the removal from aqueous medium of Orange dye (OG) considered as a model pollutant under UV radia-

tions and solar light by using indoor lab-scale reactors equipped with an artificial solar light and a larger outdoor pilot irradiated by natural solar light.

2. Experimental Details

2.1. Materials and Synthesis

Natural raw clay, involved herein, was sampled from Marrakesh-High Atlas region. Detailed characterizations performed by Rhouta *et al.* [28] on this clay revealed that it is made up of fine clay fraction (<2 μm) (>65%) along with accessory minerals, namely quartz (< 5%) and carbonates (≈ 30 wt%) in the forms of calcite ($\text{Mg}_{0.03}\text{Ca}_{0.97}\text{CO}_3$) and ankerite ($\text{Ca}_{1.01}\text{Mg}_{0.45}\text{Fe}_{0.54}(\text{CO}_3)_2$). The extracted fine fraction (<2 μm) was found to be exclusively composed of fibrous clay minerals, namely palygorskite ($\approx 95\%$) exhibiting predominant dioctahedral character and deficiency into zeolitic water along with sepiolite ($\approx 5\%$). The composition of this palygorskite was found on the basis of 26 oxygens to be $(\text{Si}_{7.97}\text{Al}_{0.03})(\text{Mg}_{2.17}\text{Al}_{1.46}\text{Fe}_{0.40}\text{Ti}_{0.05})(\text{Ca}_{0.03}\text{Na}_{0.07}\text{K}_{0.03})\text{O}_{20.18}(\text{OH})_{1.94}(\text{H}_2\text{O})_{3.88}, 2.43 \text{ H}_2\text{O}$. Its Cation Exchange Capacity (CEC), Brunauer-Emmet-Teller method (BET) specific surface area and total porous volume were assessed to be 21.2 meq $\cdot 100 \text{ g}^{-1}$, 116 $\text{m}^2\cdot\text{g}^{-1}$ and 0.458 $\text{cm}^3\cdot\text{g}^{-1}$ respectively.

The Ti precursor considered herein is the titanyl sulfate ($\text{TiOSO}_4\cdot 2\text{H}_2\text{O}$) purchased from Aldrich and used without further treatment.

In contrast to our previous works [24] [25] [26] [27] [30] in which the synthesis of clay minerals supported photocatalysts implied several laborious and time-consuming steps including purifying, homoionisation and fine fraction recovering before its functionalization, the elaboration herein was accomplished according to a one-pot route starting directly from raw clay. Indeed, given amounts of raw palygorskite clay and $\text{TiOSO}_4\cdot 2\text{H}_2\text{O}$ powders were introduced in an alumina jar of planetary ball mill PM100 from Retsch for being grinded using six alumina balls of 20 mm in diameter. The synthesis of TiO_2 supported on palygorskite fibers was achieved by *in-situ* reacting carbonates accessorially present (≈ 30 wt%) in raw clay with $\text{TiOSO}_4\cdot 2\text{H}_2\text{O}$ precursor according to different conditions. Indeed, the amount of each reactant was chosen in such a way to have a total mass of reactants of 50 g per run by considering two raw clay/ TiOSO_4 mass ratios of 0.6/1 and 3.3/1, which corresponded to mixtures in which both compounds were in stoichiometric or in excess proportions, respectively. The grinding was performed at a rate of 500 rpm for different times (10, 15, 20 and 30 min). As-grinded samples were thereafter air annealed for 1 h at different temperatures (400°C, 500°C, 600°C and 700°C). Samples were designated Pal_ $\text{TiO}_2(x)$ _G $_y$ _T $_z$ by referring to the composite nature of the sample (Pal_ TiO_2), the reactant mass ratio ($x = \text{TiO}_2/\text{Pal}$), the grinding time (G_y) and the post-heat-treatment temperature (T_z). The obtained powdered materials were finally stored for further uses.

2.2. Characterizations

The structural changes of TiO_2 upon heating of as-grinded samples were analyzed

in situ versus the temperature by XRD over the two-theta range 2_60 deg using a Bruker D8 Advance diffractometer equipped with a Vantec Super Speed detector and an Mid-Infrared (MIR) radiation heating chamber (Bragg-Brentano configuration; Ni filtered Cu K α radiation). The diffractograms were recorded every 50°C from the room temperature to 950°C. An isotherm was maintained at each level for 40 min to record the pattern then the temperature was increased using a ramp of 1 deg.s⁻¹ up to the next level. Also XRD at room temperature was recorded on TiO₂_Pal samples prior to air annealing at different temperatures in the same angular range using a Seifert XRD 3000TT diffractometer equipped with a graphite monochromator (Bragg-Brentano configuration; Cu K α radiation).

The microstructure, morphology and uniformity of the samples were analyzed at different steps of the synthesis by a Scanning Electron Microscope (SEM; Leo-435VP) equipped with an Oxford energy dispersive spectrometer (EDS, (EDS, KEVEX Si (Li) assisted software Brüker)). Also, a JEOL JEM 2010 TEM equipped with a Tracor EDS analyzer was used for characterizing clay particles and performing local elemental composition.

2.3. Photocatalytic Activity

The photocatalytic activity of different samples was evaluated using three kinds of set-ups: a laboratory-scale set-up, an indoor solar simulator and an outdoor solar pilot. As far as the first set-up is concerned, the degradation reaction was performed in a batch quartz reactor (40 × 20 × 36 mm³) placed in a thermostated chamber (25°C) under the UV light of a lamp (HPLN Philips 125 W) emitting at 365 nm. The reactor was irradiated with a photon flux of about 100 mW·cm⁻² by adjusting the distance to the lamp so that it simulates the UV intensity of solar spectrum on the earth [31]. This lamp was chosen because the OG absorption is negligible at this wavelength and, as a result, the direct photolysis of the solution (*i.e.* without photocatalyst) was found negligible for more than 24 h. The photoactivity of different samples was assessed at pH around 6 by measuring the decomposition rate of OG in aqueous solutions containing the supported photocatalyst according to a procedure previously reported [32] and adapted to the dispersion of supported powder photocatalysts in previous papers [26] [33]. The photocatalyst powder of TiO₂_Pal nanocomposites was added to 25 cm³ of OG solution (10⁻⁵ M) in an amount equal to 0.8 g·dm⁻³. This catalyst mass was found as optimum to avoid excess of catalyst and to ensure an efficient absorption of photons [34]. The dispersion was agitated with an inert Teflon magnetic stirrer. To determine the dye concentration, aliquots were taken from the mixture at regular time intervals and centrifuged at 12,500 rpm for 5 min. The OG concentration in the supernatant was determined by measuring the absorbance at 480 nm using a UV-VIS-NIR spectrophotometer (Perking Elmer lambda 19).

Sunlight is particularly weak in the UV spectral region and, in addition, it changes along the day due to day-night and seasonal cycles [35] [36]. Thus, prior

optical and kinetic studies have to be performed to determine on one hand optimal catalyst mass allowing the maximum ($\approx 90\%$) of the absorption of photons (considered as reactant) and, on the other hand, kinetic constants to achieve process efficiency in an outdoor solar pilot [35] [37] [38]. Therefore, optical properties of photocatalysts suspensions differing in mass concentrations were studied by an optical experimental setup described in details elsewhere [37] [39]. Practically, the light supplied by a source simulating solar radiation (maximum intensity equal to $1000 \text{ W}\cdot\text{m}^{-2}$ in the full spectral range, *i.e.* $50 \text{ W}_{\text{uv}}\cdot\text{m}^{-2}$ in the UV range) came across a Polymethyl methacrylate (PMMA treated to be UVA transparent, Sunactive[®] GS2458) cell 2 cm thick (*i.e.* optical length) containing under stirring the TiO_2 _Pal dispersions whose concentrations ranged from 0.1 to $4 \text{ g}\cdot\text{L}^{-1}$. This cell was placed at the inlet of an integrating sphere. The direct radiation as well as scattered radiation transmitted hence collected from the integration sphere were directed via an optical fiber towards a spectrophotometer permitting the detection of wavelengths ranging from 250 to 1100 nm (ultraviolet, visible and near-infrared). The transmission of light was hence assessed versus catalyst powder concentration to determine the mass concentration at which the 90% absorbency was reached. Afterwards, kinetic study of OG dye degradation was carried out versus mass concentration of catalysts powders dispersion by using an indoor solar simulator set-up. For a given mass concentration, the catalyst dispersion was kept under stirring in a 150 mL quartz bucket (suspension height of 5 cm), then it was irradiated by sunlight simulator ($1000 \text{ W}\cdot\text{m}^{-2}$) under constant photons flow. At different time intervals, aliquots were picked up from media, centrifuged and resulting supernatants analyzed by spectrophotometry to determine the dye concentration according to the way described above.

Afterwards, the efficiency of TiO_2 _Pal catalysts towards the photodegradation under sunlight of OG dye was tested by using an outdoor solar pilot described in details by Janin *et al.*, [40] (picture given in the supplementary Figure 1S.). Briefly, a mass concentration of TiO_2 _Pal that permitting 90% of photons absorption was dispersed under stirring in an OG dye solution and stored in a stainless-steel tank (with a maximum volume of 50 L). Then 6 L of effluent were fed into a flat solar panel ($30 \times 100 \times 2 \text{ cm}^3$) from the bottom to the top via a liquid pump and recirculated into the tank. This panel was covered with a special PMMA plate to prevent evaporation of compounds and to ensure watertight. This flat reactor was oriented southwards and inclined at an angle around 42° in order to maximize the average solar irradiation throughout the year. This was controlled by two equipments: a pyranometer whose wavelength domain varies between 380 to 2800 nm and an UV radiometer (UVA-Sensor CT-UVA 3) measuring the corresponding spectrum in the range of 310 - 400 nm.

3. Results and Discussion

3.1. Structural Characterizations

Figure 1 shows an overview of the room temperature XRD diagrams of the two

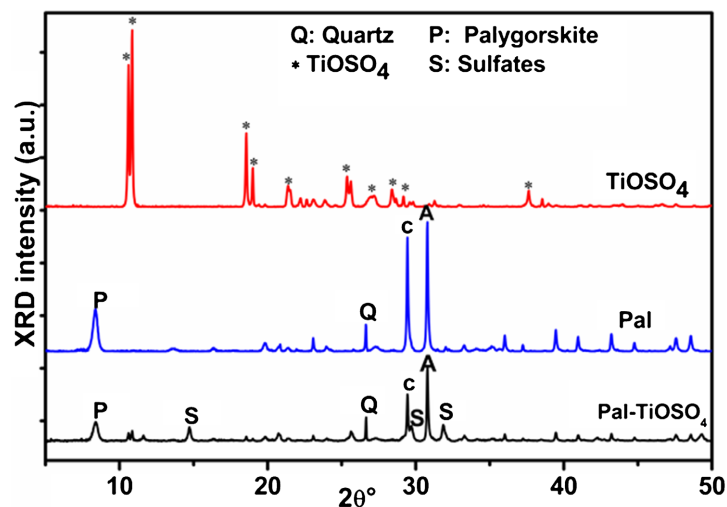


Figure 1. Room temperature XRD patterns of TiOSO_4 , raw clay (Pal) and Pal- TiOSO_4 mixture in mass ratio of 0.6/1 after grinding of each of these samples at 500 rpm for 30 minutes.

starting materials after a grinding for 30 min at 500 rpm: titanium oxysulfate precursor (TiOSO_4) and palygorskite-rich raw clay (Pal). Also, the XRD diagrams of a mixture of TiOSO_4 and Pal clay in a mass ratio of 0.6/1 after grinding for 30 min at 500 rpm is reported (Pal- TiOSO_4).

The diffractogram pertaining to the milled titanium precursor revealed only the reflections at the 2θ angular positions of 10.67° (8.35 Å), 10.95° (8.20 Å), 18.61° (4.79 Å), 19.07° (4.69 Å), 21.43° (4.16 Å), 25.44° (3.50 Å), 25.70° (3.47 Å), 28.47° (3.13 Å), 29.25° (3.05 Å), 37.70° (2.38 Å), 38.61° (2.33 Å) corresponding to the compound TiOSO_4 (ICDD file N°14-503) without evidence for the formation of any other crystalline phase, especially TiO_2 . In the same sense, the XRD pattern of the grinded Pal raw clay showed several reflections corresponding to the fibrous mineral, *i.e.* palygorskite, at the angular positions described by Rhouta *et al.*, [30]. The characteristic basal reflection is at $2\theta \approx 8.38^\circ$ (10.56 Å) in addition to the peaks ascribed to the accessory minerals, namely the carbonates in the form of calcite (C) $\text{Mg}_{0.03}\text{Ca}_{0.97}\text{CO}_3$ (ICDD file: 01-089-1304) and ankerite (A) $\text{Ca}_{1.01}\text{Mg}_{0.45}\text{Fe}_{0.54}(\text{CO}_3)_2$ (ICDD: 01-084-20 2066) as well as quartz (Q) (ICDD file: 03-065-0466) whose strongest reflections were observed at 29.46° (3.03 Å), 30.82° (2.90 Å) and 26.64° (3.34 Å), respectively.

This result showed that both the palygorskite and the accessory phases, constituting the raw Pal clay, were apparently not affected by the grinding operation in the mechanosynthesis jar since their crystallographic structure remained stable. On the other hand, these grinding conditions of the Pal- TiOSO_4 mixture caused a drastic decrease in the XRD intensities of TiOSO_4 reflexions at the point to disappear, as well as those of the carbonates (calcite and ankerite), while preserving the clay structure confirmed by the persistence of the corresponding peaks. The disappearance of TiOSO_4 reflexions can be due to its amorphisation but the major event during grinding is the trigger of reaction (1), according to

which TiOSO_4 reacts with the carbonates present among the accessory minerals in the raw clay Pal:



The occurrence of this reaction was further confirmed by the production of the hydrated sulfate compound $\text{CaSO}_4 \cdot 0.5\text{H}_2\text{O}$ evidenced by the presence in the composite sample Pal_ TiOSO_4 of the characteristic peaks noted S on the diffractogram (Figure 2) at angular positions 2θ of 14.71° (6.00 nm), 29.71° (3.00 nm) and 31.86° (2.80 nm) in agreement with the ICDD file 01-081-1848. The near-consumption of the TiOSO_4 precursor revealed by XRD may be due to the fact that the low value of the mass ratio TiOSO_4 :clay (0.6:1) would be the driving force of reaction (1).

Furthermore, the reaction (1) also showed that titanium dioxide has to be formed but no diffraction peaks of this oxide was observed in Figure 3 suggesting that the as-prepared TiO_2 phase must be amorphous after the mechano-synthesis step (TiOSO_4 : clay = 0.6:1; 500 rpm; 30 min). Subsequently, a mixture of TiOSO_4 and Pal raw clay with the mass ratio 3.3/1, i.e. with Ti precursor in excess was grinded for 30 min at 500 rpm. Then, XRD patterns of this composite sample were recorded *in-situ* in air as a function of the temperature (Figure 2).

For as-milled sample, the diagram recorded at 50°C revealed that, as mentioned above, amorphous TiO_2 and the hydrated CaSO_4 product were formed during the grinding stage as a result of the above reaction (1). In this respect, a significant proportion of the carbonates were consumed by the reaction with TiOSO_4 (that was in excess) has shown by the decrease of their XRD intensity. This was further supported by a huge decrease in carbonate content determined

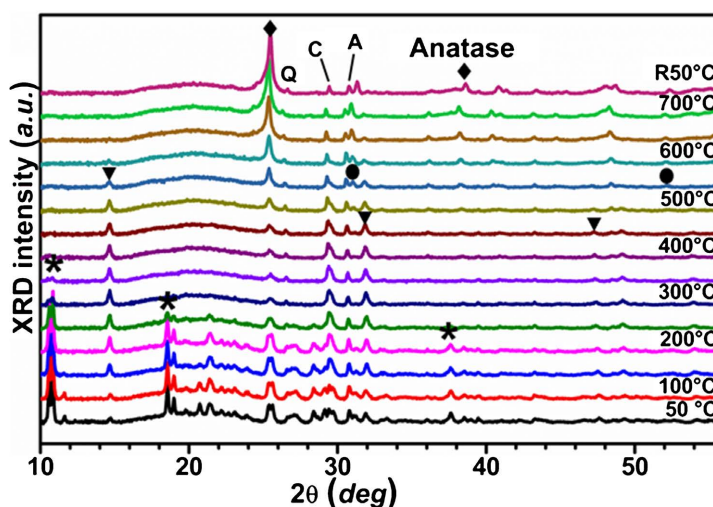


Figure 2. X-ray diffractograms recorded *in-situ* in air as a function of the sample temperature of a TiOSO_4 /Pal (3.3/1) mixture after mechano-synthesis (Step 1). These diagrams were recorded every 50°C ; they represented the effect of calcination as 2nd step of the synthesis process. They showed the main compounds that disappeared were TiOSO_4 (★), calcite (C), ankerite (A), while the compounds that formed were $\text{CaSO}_4 \cdot x\text{H}_2\text{O}$ (▼), CaSO_4 (●), TiO_2 anatase (♦), and the most thermally stable accessory compounds like quartz (Q).

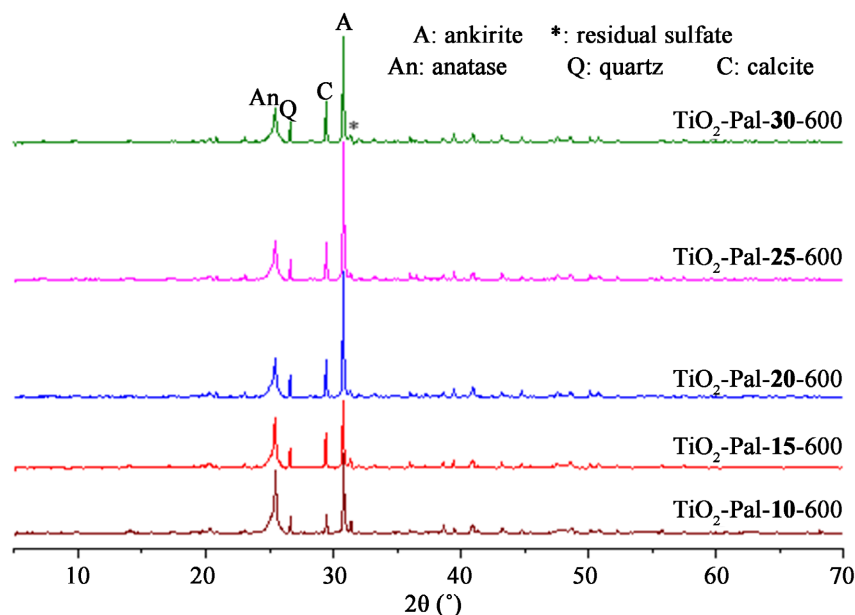


Figure 3. Stacking of XRD patterns of TiO_2 -Pal photocatalysts prepared by grinding TiOSO_4 and Pal raw clay in a mass ratio of 0.6/1 during 10, 15, 20, 25 and 30 min at 500 rpm.

by coulometric analysis. Indeed, the carbonate content has been reduced approximately by a factor of 2, from 28 wt% \pm 2 wt% in the raw clay Pal to 13 wt% \pm 2 wt% in the grinded TiOSO_4 /Pal (3.3/1) mixture.

By increasing the temperature, it can be seen that the crystallization of anatase TiO_2 started from 450°C as shown by the emergence of the corresponding peaks at angular positions 2θ of about 25.44° (3.51 Å) and 38.53° (2.33 Å) (ICDD Data Sheet 01-021-1272). As the temperature increased further, the anatase peaks became more intense and well resolved, indicating the improvement of its crystallization. The anatase peaks remained observable up to 700°C, without the appearance of any XRD peaks of the less photoactive rutile variety. This strongly denoted the remarkable stability of the anatase formed under the conditions of this study. Palygorskite peaks were observable up to 400°C, beyond which their intensities severely reduced. This can be ascribed to the occurrence of structural collapse of the clay mineral. However, this can be also due to an absorption filter induced by the conformal coverage of anatase particles on palygorskite fibers as suggested by Rhouta *et al.*, [28] and Bouna *et al.*, [29] and confirmed by the TEM analyses shown in the next section.

In order to examine the effect of grinding time on the reactivity of TiOSO_4 with the carbonates present in the Pal raw clay, a mixture of the two compounds in a ratio of 0.6/1 was ground at 500 rpm for 10, 15, 20, 25 and 30 min and then air annealed at 600°C for 1 h. The superimposition of the corresponding XRD diagrams (Figure 3) clearly showed the formation of anatase TiO_2 for all the samples investigated regardless grinding time. Nevertheless, the anatase crystallinity appeared to improve with the grinding time as evidenced by the gradual narrowing of its characteristic peak at about 2θ around 25°. In this respect, by re-

ferring to quartz, which is an insensible and stable accessory mineral under the applied grinding conditions, the increase of the intensity ratio of the main anatase/quartz peaks is noteworthy. This probably reflected an increase in the amount of anatase phase formed with the increase of grinding time.

3.2. Microstructural Characterizations

XRD results were further supported by TEM characterizations. Indeed, depending on the grinding conditions, TEM analysis after the first step showed palygorskite fibers of 30 - 70 nm in diameter and 650 nm in length mixed with TiOSO_4 platelets of 400 - 600 nm with an average thickness of 3 - 5 μm . At this stage, no evidence for crystallized anatase nanoparticles (NPs) was found confirming this oxide phase was amorphous. After annealing at 600°C in air for 1 h, TEM revealed that palygorskite fibers were entirely wrapped with homogeneous monodisperse and spherical TiO_2 anatase NPs 10 - 15 nm in diameter (**Figure 4(a)**). Only a few palygorskite fibers were not covered as revealed by EDS analysis. For most of them, a granular and conformal TiO_2 coverage formed a uniform cladding (**Figure 4(b)**).

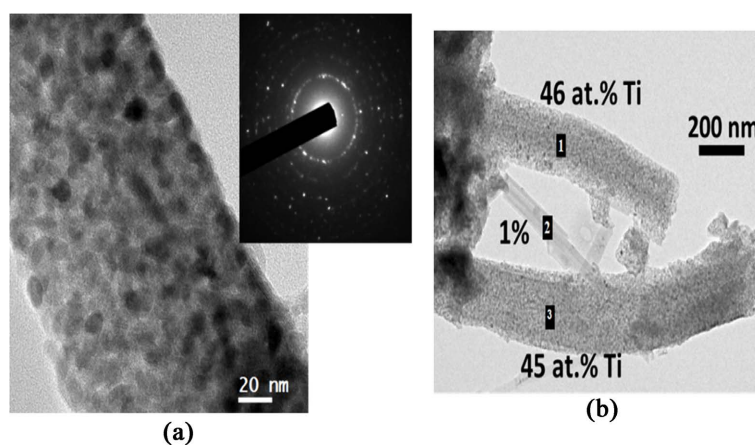


Figure 4. TEM micrographs and corresponding electron diffraction pattern indexed as TiO_2 anatase (a) and EDS local analysis showing uncoated (point 2) and uniformly coated point 1 and 3) palygorskite fibers (b).

3.3. Photocatalytic Properties under UV Light

The photocatalytic activity of different TiO_2 -Pal composite samples elaborated by mechanosynthesis was tested towards the degradation under UV light of OG dye by using the laboratory set-up described in the experimental section (2.3). The results in **Figure 5** showed that photocatalytic efficiency significantly increased with the amount of TiOSO_4 used in photocatalyst synthesis and thus the amount of TiO_2 present in TiO_2 -Pal nanocomposite. This was evidenced by on one hand the strong decrease of OG concentration for instance in the first 10 min, revealing a high initial degradation rate of the pollutant around $2.6 \times 10^{-2} \text{ s}^{-1}$ for TiO_2/Pal mass ratio of 3.3/1 with respect to that determined for the mass ratio of 0.6/1 ($\approx 1.5 \times 10^{-2} \text{ s}^{-1}$). On the other hand, the almost total elimination of

the OG dye from the solution was achieved within about 2 h when using TiO_2/Pal mass ratio of 3.3/1 whilst almost 10% of the dye remained after the same time of UV irradiation in presence of TiO_2/Pal mass ratio of 0.6/1 (but a plateau has not yet been reached).

The influence of annealing temperature on the photocatalytic activity towards the removal of OG dye of TiO_2/Pal was afterwards studied on the most active one corresponding to TiO_2/Pal mass ratio = 3.3/1. **Figure 6** interestingly showed that the unheated as-milled Pal-TiOSO_4 mixture (sample $\text{Pal-TiO}_2(3.3)_{30}$) already exhibited photoactivity under UV irradiation. Indeed, 50% of the initial quantity of OG decreased after 2 hours of irradiation. This is due to the formation

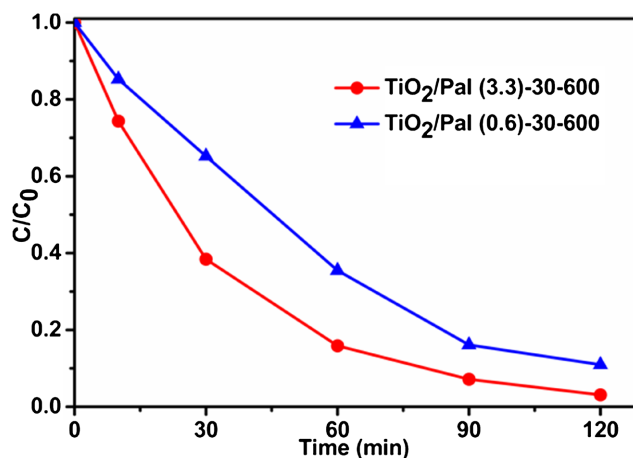


Figure 5. Change in the concentration of OG (where C_0 and C denote the concentrations of OG at the initial time $t = 0$, and after an elapsed time t of the photocatalytic reaction) vs. UV irradiation time of the samples, differing in $\text{TiOSO}_4/\text{Pal}$ mass ratio (0.6/1 and 3.3/1), grinded during 30 min at 500 rpm and afterwards air annealed at 600 °C for 1 h.

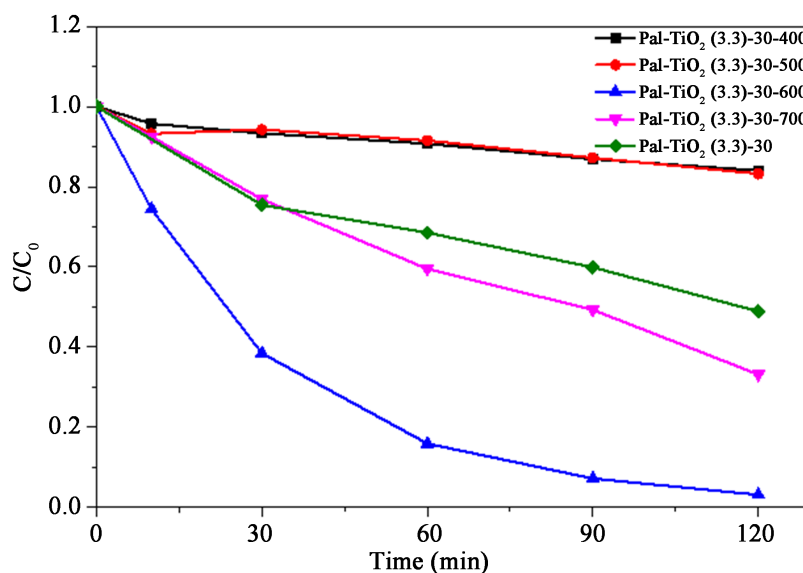


Figure 6. Change in the concentration of OG vs. UV irradiation time of TiO_2/Pal elaborated by mechanosynthesis ($\text{TiOSO}_4/\text{Pal}$ mass ratio = 3.3/1, grinding at 500 rpm for 30 min) and air annealing at 400 °C, 500 °C, 600 °C and 700 °C.

of photoactive TiO₂ resulting, as beforehand mentioned, from the heterogeneous solid-state reaction between TiOSO₄ and the carbonate phases (calcite + ankerite) present as accessory minerals in the Pal raw clay (reaction 1). Although the TiO₂ formed in as-grinded material was amorphous, as ascertained above by XRD, this is not exceptional since it was already shown that amorphous TiO₂ can be active in photocatalysis under UV irradiation [41]. Indeed, from a general point of view, even if amorphous semiconductors have less efficient electronic properties than their crystallized counterparts, they nevertheless find specific applications as in photovoltaic.

Samples annealed at 400°C and 500°C showed quite similar photo-degradation curves of the OG and paradoxically showed a lower photoactivity compared to as-grinded sample, allowing the removal of only 15% after 2 hours of illumination. This annealing temperature range is therefore insufficient to ensure a good crystallization of TiO₂ in the form of anatase but, on the other hand, it seems to be sufficient for inducing a detrimental diffusion of species that trap excitons (Pal clay cations for example), thus affecting the photocatalytic efficiency of the composite. Calcination at 600°C promoted the most efficient active palygorskite-supported TiO₂ photocatalyst since it allowed almost complete degradation of the OG after 2 hours of UV irradiation. This improvement was attributed to the good crystallinity of TiO₂ anatase upon the sample calcination at 600°C as confirmed above by XRD. On the other hand, when the sample was annealed at 700°C, photocatalytic activity again decreased. This reduction in photocatalytic activity may be due to the growth of TiO₂ particles beyond the optimal nanocrystalline size, which promotes the recombination of charge carriers. Also, a partial phase transformation of the more active anatase TiO₂ phase into the less photoactive rutile variety as reported by Bouna *et al.*, [29] and Rhouta *et al.*, [28] is not excluded although none of the corresponding peaks have yet been detected at 700°C, the presence of other crystalline phases can hide them.

3.4. Photocatalytic Properties under Sunlight

Owing to its high photoactivity under UV evidenced above by the tests on the laboratory set-up, the TiO₂-Pal nanocomposite with mass ratio TiO₂/Pal of 3.3/1 was thereafter retained for performing the study of photocatalytic activity under sunlight towards the removal of OG dye.

3.4.1. Activity under Constant Solar Irradiation – Indoor Experiments

For studying optical properties of TiO₂-Pal, the change in transmittance (%), defined as the ratio of transmitted (I_t) to incident (I_i) intensities, was followed versus catalyst slurry mass concentration. **Figure 7** showed that the necessary amount for the absorption of 90% of incident light simulating sunlight (1000 W/m²) for a catalyst dispersion thickness of 2 cm (C_{2cm}) was around 2.36 g/L, *i.e.* 1.34 g/L of TiO₂ taking into account its proportion of 57 wt% assessed by Individual Counting by single Particle (ICP) in the nanocomposite. Photocatalytic tests in batch mode using the indoor solar simulator described in the experi-

mental section were performed by varying the amount of $\text{TiO}_2\text{-Pal}$ dispersed in OG solution of 5 cm of thickness around the optimum amount ($C_{5\text{cm}} = 2/5 \times C_{2\text{cm}} \approx 0.95$ g/L) allowing maximum absorption.

Figure 8 showed that very low amount of $\text{TiO}_2\text{-Pal}$, e.g. 0.25 g/L, exhibited a relatively low photocatalytic activity leading to the removal of about 40% of OG after 150 min of irradiation with an initial photo-degradation rate of about $5 \times 10^{-3} \text{ s}^{-1}$. Nevertheless, by increasing the $\text{TiO}_2\text{-Pal}$ mass concentration beyond 0.5 g/L up to 1.5 g/L, a better efficiency occurs and a quite similar photocatalytic behavior of the photocatalyst towards OG elimination was observed. Indeed, the OG photodegradation considerably increased as evidenced on one hand, by the strong decrease of OG concentration for instance in the first 20 min, revealing a high initial degradation rate ($\approx 7 \times 10^{-3} \text{ s}^{-1}$) of the pollutant and, on the other

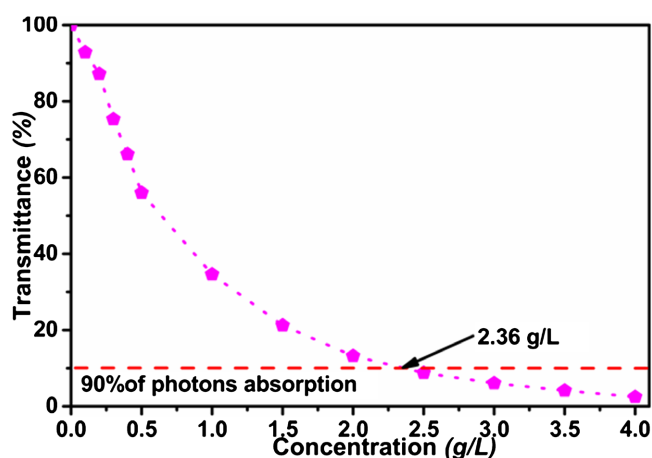


Figure 7. Variation of transmittance in the spectral range 250 - 1100 nm (artificial solar light $1000 \text{ W}\cdot\text{m}^{-2}$) as a function of the catalyst dispersion concentration in an aqueous suspension.

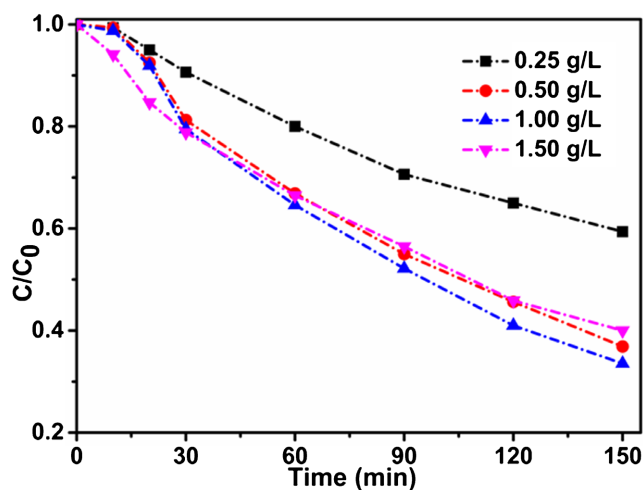


Figure 8. Variation of the relative OG concentration versus time (where C_0 and C denote the OG concentrations at the initial time $t = 0$, and after an elapsed time t) in the $1000 \text{ W}\cdot\text{m}^{-2}$ solar simulator recorded for different mass concentrations of the $\text{TiO}_2\text{-Pal}$ composite photocatalyst.

hand, by the elimination of almost 60% of OG dye from the solution within the same time of irradiation. These results showed that around the optimal mass concentration of $\text{TiO}_2\text{-Pal}$ (≈ 0.95 g/L) beforehand determined by optical measurements, the catalyst exhibited maximal photoactivity for dye removal due to highest light absorption. Thus, an increase in the mass concentration of the photocatalysts beyond its optimal mass concentration is unnecessary since the maximum absorption of incident light has already been reached. This is in agreement with Plantard *et al.*, [42] who reported that for a given pollutant and a fixed initial concentration, the degradation kinetic constants obtained for the same photocatalyst depended solely on the quantity of photons absorbed. As a result, degradation by photocatalysis is function to the concentration of the catalyst in suspension, up to a threshold value at which all the incident radiation is almost absorbed.

Besides photocatalyst mass concentration in the aqueous suspension, photons fluxes also constituted a crucial parameter influencing heterogeneous photocatalysis process especially under solar light characterized by the variation of irradiation intensity. **Figure 9**, representing OG proportion change versus solar irradiation time at different photons fluxes in presence of 0.94 g/L of $\text{TiO}_2\text{-Pal}$ revealed that in general, and as expected, an increase of the radiation intensity led to an increase of the OG pollutant degradation. This is the result of the increase of quantity of photons absorbed. It is obviously well known that this is only the UV part of the solar spectrum that is effective for photocatalytic treatment with TiO_2 as active component. With the solar simulator UV intensity is directly proportional to the total intensity delivered by the lamp. It is almost the case for solar natural irradiation (even if the UV percentage is influenced by the weather conditions). So, we made the choice to keep the total radiation intensity received as the reference. It is the energy flux received by the surface of a reactor working in outdoor conditions.

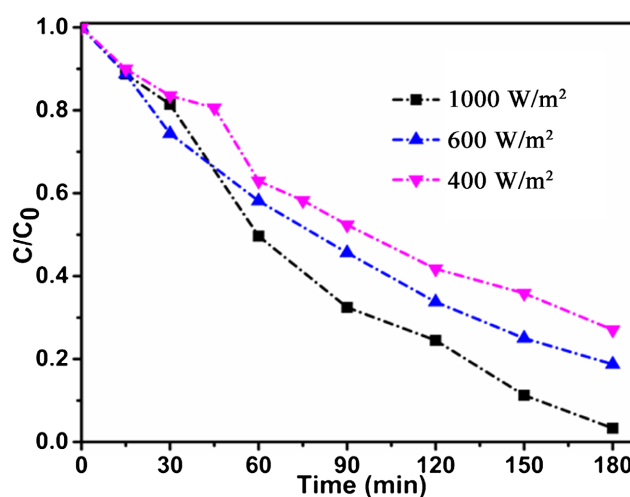


Figure 9. Variation of the OG proportion versus time (s) upon irradiation simulating sunlight at 400, 600 and 1000 $\text{W}\cdot\text{m}^{-2}$ in presence of $\text{TiO}_2\text{-Pal}$ (0.94 g/L) composite photocatalyst.

For being transposed to solar photocatalysis treatment, OG photodegradation kinetic should be modulated taking into account the irradiation intensity key parameter. In photodegradation of a target molecule (OG herein) using a slurry catalyst (TiO₂_Pal), rates can be approached by the modified Langmuir-Hinshelwood (L-H) relationship (1) [21]:

$$\frac{dC}{dt} = k(I) \frac{C}{1 + \beta \cdot C} = - \left(\alpha \cdot \frac{S}{V_T} \cdot I \right) \frac{C}{1 + \beta \cdot C} \quad (1)$$

With $k(I)$ the apparent kinetic constant (s⁻¹) function of the intensity, C the OG concentration (g·L⁻¹), β (L·g⁻¹) a constant determined by comparison between calculated and experimental data. In the simplest case, $k(I)$ is directly proportional to the intensity I received by unit volume of solution (V_T in L) with an irradiated surface S (m²). α (J·L⁻¹) is the second unknown parameter. If necessary, a dependence of k according to a law in power of the irradiation can be introduced to account of additional limiting phenomena such as the charge recombination.

For a constant irradiation intensity, the integration of Equation (1) leads to the expression (2):

$$f\left(\frac{C}{C_0}, \beta\right) = \ln\left(\frac{C}{C_0}\right) + \beta \cdot C_0 \cdot \left(\frac{C}{C_0} - 1\right) = -k(I) \cdot t \quad (2)$$

To be valuable, the value of β has to be constant whatever is the irradiation. It is determined simply by considering the left part of equation 2 depends linearly on time. **Figure 10** depicted experimental profiles of the logarithmic adimensional concentration C/C_0 as a function of the time with a value of $\beta = 0.65$ L·g⁻¹. It showed linear dependence with a satisfactory agreement. This ascertained pseudo first-order kinetics whose the slope k depends on the intensity of the

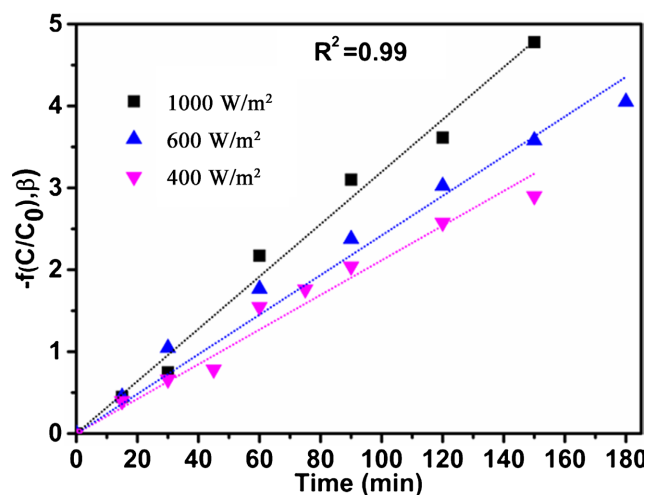


Figure 10. Linear variation of $\ln(C/C_0)$ of OG versus time (s) for different irradiation intensities simulating sunlight in the presence of 0.94 g/L of TiO₂_Pal catalyst for $\beta = 0.65$ L·g⁻¹ confirming a pseudo first order kinetics. Continuous colored lines represent the best agreement between the experimental data and a linear regression for each level of irradiation.

irradiation according to the relationship (3).

$$k(I) = \frac{S}{V_T} \cdot \alpha \cdot I \quad (3)$$

Likewise, the variation of the apparent kinetic constant k versus irradiation intensity (I) (Figure 11) showed a linear trend supported by a reasonable degree of accuracy of about 0.99. Hence, the value of the kinetic constant (α), deduced from the slope, can be assessed to be around 1.5 L/kJ.

By introducing the values of α and β in the expression (2), the C/C_0 plots versus time show a very good fitting between the experimental and simulated data for all irradiation flux densities, as expected from the good agreement already reported in Figure 10 and Figure 11. This result validates the proposed kinetic model described by equation (2).

3.4.2. Activity under Natural Discontinuous Irradiation - Outdoor Solar Pilot

The photocatalytic tests for the removal of OG dye from aqueous solution were carried out in presence of TiO₂_Pal slurry by using an outdoor solar pilot and according to conditions described in the experimental section (2.3). Nonetheless, owing to the variation of solar irradiation along a day, the change of OG dye during these tests should be versus the cumulative energy Q_g (J·L⁻¹) received by the reactor given by the relationship (4) [26]:

$$Q_g = \frac{S}{V_T} \cdot \int_0^{t_i} I(t) dt \quad (4)$$

With t_i (s) the time at which an aliquot was taken for being centrifuged and analyzed by the spectrophotometer and $I(t)$ the solar irradiation intensity measured over time using the sensors mounted on the pilot as described in the experimental section.

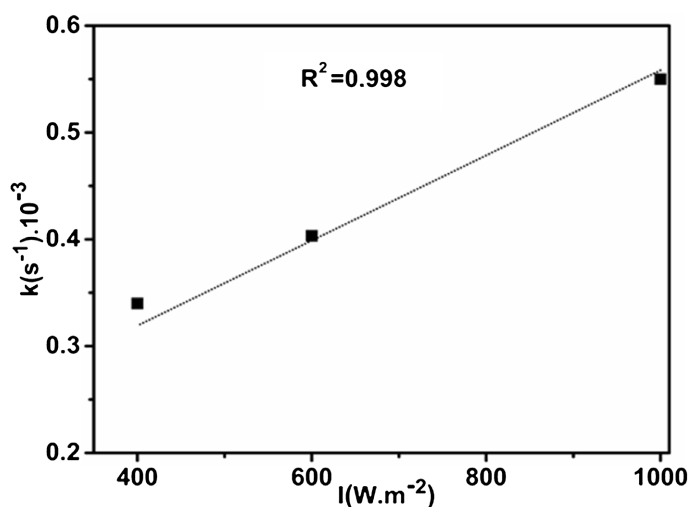


Figure 11. Linear variation of the kinetic constant k of OG photodegradation versus the irradiation intensity I simulating sunlight onto TiO₂_Pal photocatalyst slurry. The continuous gray line simulates the data according to equation (3).

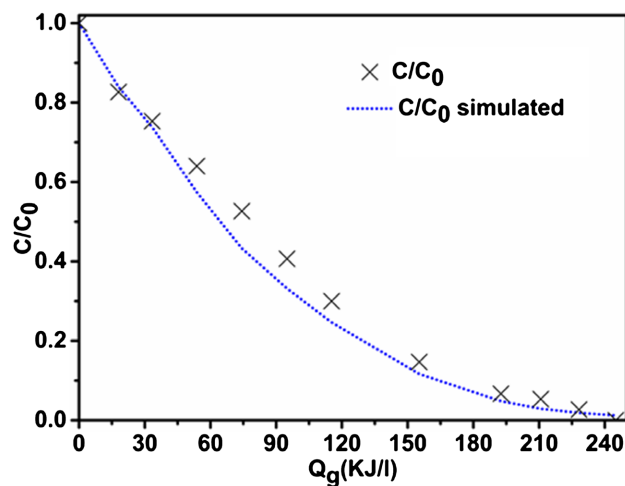


Figure 12. Change of the experimental relative concentration of the OG (×) and simulated data (dotted curve) versus the total cumulated energy obtained for TiO₂_Pal composite photocatalyst.

Figure 12 shows, like data obtained with the indoor solar simulator in “batch” mode, a decrease in OG dye proportion upon solar irradiation, which thus confirms the photoactivity of TiO₂_Pal under solar light. In this respect, 50% of the OG dye was removed with a cumulated energy of 74.2 kJ/L whilst the total removal of the dye required a cumulated energy of 250 kJ/L.

Besides, by introducing the numerical values of α (1.5 L/kJ) and β (0.65 L·g⁻¹) beforehand determined in the relationship (5) derived from the above one (2) after substituting $I(t)$ by $Q_g(t)$, a good agreement between simulated and experimental data was observed with a good degree of accuracy.

$$\frac{C(t)}{C_0} = e^{-\left[\alpha \frac{S}{V_T} Q_g(t) + \beta C_0 \left(\frac{C}{C_0} - 1\right)\right]} \quad (5)$$

This confirmed the validation of the kinetic model proposed and ascertained that the OG photodegradation in presence of TiO₂_Pal slurry was of first order with a kinetic constant of 1.5 L/kJ and did not involve adsorption phenomenon.

4. Conclusions

TiO₂ photocatalyst supported onto natural palygorskite clay mineral fibers (TiO₂_Pal) was successfully elaborated by a one-pot dry mechanical method. This elaboration process is very interesting because it directly uses palygorskite clay without the multiple purification steps that wet processes frequently require. Furthermore, it is solvent free, eco-friendly and based on smart *in situ* solid-state reaction between carbonates accessory minerals contained in the raw clay and a cheap molecular Ti precursor. As a result, it can be easily scaled up to an economically viable large-scale production.

Structural analysis and microstructural characterization using XRD and TEM respectively showed that TiO₂_Pal, revealed homogeneous monodisperse TiO₂ NPs in the form of anatase wrapping palygorskite fibers. This sample was shown

to be the most photoactive under UV irradiation towards the removal of OG dye from aqueous solution upon the use of a laboratory set-up. Then photocatalytic tests carried out by an indoor solar simulator set-up on OG dye solution containing an optimal mass concentration of TiO₂_Pal nanocomposite were found to assure the maximum of the elimination of OG. In this respect, a good agreement was demonstrated between experimental and simulated data using a pseudo first order kinetic model for the dye photodegradation. The same photocatalytic behavior was also obtained with an outdoor solar pilot confirming the photoactivity of these supported TiO₂_Pal photocatalysts under sunlight.

Acknowledgements

The financial supports from the “Programme d'Action Intégrée Volubilis” (N° 14/SM/14) and the Project of PPR-CNRST “Domaines Prioritaires de la Recherche Scientifique et du Développement Technologique” (PPR1/2015/63) are gratefully acknowledged.

Conflicts of Interest

The authors declare no conflicts of interest regarding the publication of this paper.

References

- [1] Robertson, P.K.J. (1996) Semiconductor Photocatalysis: An Environmentally Acceptable Alternative Production Technique and Effluent Treatment Process. *Journal of Cleaner Production*, **4**, 203-212. [https://doi.org/10.1016/S0959-6526\(96\)00044-3](https://doi.org/10.1016/S0959-6526(96)00044-3)
- [2] Herrmann, J. (1999) Heterogeneous Photocatalysis: Fundamentals and Applications to the Removal of Various Types of Aqueous Pollutants. *Catalysis Today*, **53**, 115-129. [https://doi.org/10.1016/S0920-5861\(99\)00107-8](https://doi.org/10.1016/S0920-5861(99)00107-8)
- [3] Fujishima, A., Rao, T.N. and Tryk, D.A. (2000) Titanium Dioxide Photocatalysis. *Journal of Photochemistry and Photobiology C: Photochemistry Reviews*, **1**, 1-21. [https://doi.org/10.1016/S1389-5567\(00\)00002-2](https://doi.org/10.1016/S1389-5567(00)00002-2)
- [4] Fujishima, A. and Zhang, X. (2006) Titanium Dioxide Photocatalysis: Present Situation and Future Approaches. *Comptes Rendus Chimie*, **9**, 750-760. <https://doi.org/10.1016/j.crci.2005.02.055>
- [5] Paz, Y. (2006) Preferential Photodegradation—Why and How? *Comptes Rendus Chimie*, **9**, 774-787. <https://doi.org/10.1016/j.crci.2005.03.032>
- [6] Carp, O. (2004) Photoinduced Reactivity of Titanium Dioxide. *Progress in Solid State Chemistry*, **32**, 33-177. <https://doi.org/10.1016/j.progsolidstchem.2004.08.001>
- [7] Ghosh Chaudhuri, R. and Paria, S. (2014) Visible Light Induced Photocatalytic Activity of Sulfur Doped Hollow TiO₂ Nanoparticles, Synthesized via a Novel Route. *Dalton Transactions*, **43**, 5526-5534. <https://doi.org/10.1039/c3dt53311e>
- [8] Alvarez Lemus, M.A., Monroy, H., López, T., De la Cruz Hernández, E.N. and López-González, R. (2016) Effect of Surface Modification on the Bioactivity of Sol-Gel TiO₂-Based Nanomaterials. *Journal of Chemical Technology & Biotechnology*, **91**, 2148-2155. <https://doi.org/10.1002/jctb.4915>
- [9] Marien, C.B.D., Marchal, C., Koch, A., Robert, D. and Drogui, P. (2017) Sol-Gel

- Synthesis of TiO₂ Nanoparticles: Effect of Pluronic P123 on Particle's Morphology and Photocatalytic Degradation of Paraquat. *Environmental Science and Pollution Research*, **24**, 12582-12588. <https://doi.org/10.1007/s11356-016-7681-2>
- [10] Moiseev, A., Krichevskaya, M., Qi, F., Weber, A.P. and Deubener, J. (2013) Analysis of Photocatalytic Performance of Nanostructured Pyrogenic Titanium Dioxide Powders in View of Their Polydispersity and Phase Transition: Critical Anatase Particle Size as a Factor for Suppression of Charge Recombination. *Chemical Engineering Journal*, **228**, 614-621. <https://doi.org/10.1016/j.cej.2013.05.038>
- [11] Mamaghani, A.H., Haghghat, F. and Lee, C.S. (2019) Hydrothermal/Solvothermal Synthesis and Treatment of TiO₂ for Photocatalytic Degradation of Air Pollutants: Preparation, Characterization, Properties, and Performance. *Chemosphere*, **219**, 804-825. <https://doi.org/10.1016/j.chemosphere.2018.12.029>
- [12] Umebayashi, T., Yamaki, T., Itoh, H. and Asai, K. (2002) Band Gap Narrowing of Titanium Dioxide by Sulfur Doping. *Applied Physics Letters*, **81**, 454. <https://doi.org/10.1063/1.1493647>
- [13] Umebayashi, T., Yamaki, T., Yamamoto, S., Miyashita, A., Tanaka, S., Sumita, T. and Asai, K. (2003) Sulfur-Doping of Rutile-Titanium Dioxide by Ion Implantation: Photocurrent Spectroscopy and First-Principles Band Calculation Studies. *Journal of Applied Physics*, **93**, 5156-5160. <https://doi.org/10.1063/1.1565693>
- [14] Billik, P., Plesch, G., Brezová, V., L'Kuchta, L., Valko, M. and Mazúr, M. (2007) Anatase TiO₂ Nanocrystals Prepared by Mechanochemical Synthesis and Their Photochemical Activity Studied by EPR Spectroscopy. *Journal of Physics and Chemistry of Solids*, **68**, 1112-1116. <https://doi.org/10.1016/j.jpics.2007.02.010>
- [15] Billik, P. and Plesch, G. (2007) Mechanochemical Synthesis of Anatase and Rutile Nanopowders from TiOSO₄. *Materials Letters*, **61**, 1183-1186. <https://doi.org/10.1016/j.matlet.2006.06.080>
- [16] Čaplavičová, M., Billik, P., Čaplavič, L., Brezová, V., Turáni, T., Plesch, G. and Fejdi, P. (2012) On the True Morphology of Highly Photoactive Anatase TiO₂ Nanocrystals. *Applied Catalysis B: Environmental*, **117-118**, 224-235. <https://doi.org/10.1016/j.apcatb.2012.01.010>
- [17] Houari, M., Saidi, M., Tabet, D., Pichat, P. and Khalaf, H. (2005) The Removal of 4-Chlorophenol and Dichloroacetic Acid in Water Using Ti-, Zr- and Ti/Zr-Pillared Bentonites as Photocatalyst. *The American Journal of Applied Sciences*, **2**, 1136-1140. <https://doi.org/10.3844/ajassp.2005.1136.1140>
- [18] Liu, J., Dong, M., Zuo, S. and Yu, Y. (2009) Solvothermal Preparation of TiO₂/Montmorillonite and Photocatalytic Activity. *Applied Clay Science*, **43**, 156-159. <https://doi.org/10.1016/j.clay.2008.07.016>
- [19] Nieto-Suárez, M., Palmisano, G., Ferrer, M.L., Gutiérrez, M.C., Yurdakal, S., Augugliaro, V., Pagliaro, M. and del Monte, F. (2009) Self-Assembled Titania-Silica-Sepiolite Based Nanocomposites for Water Decontamination. *Journal of Materials Chemistry*, **19**, 2070. <https://doi.org/10.1039/b813864h>
- [20] An, T., Chen, J., Li, G., Ding, X., Sheng, G., Fu, J., Mai, B. and O'Shea, K.E. (2008) Characterization and the Photocatalytic Activity of TiO₂ Immobilized Hydrophobic Montmorillonite Photocatalysts: Degradation of Decabromodiphenyl Ether (BDE 209). *Catalysis Today*, **139**, 69-76. <https://doi.org/10.1016/j.cattod.2008.08.024>
- [21] Aranda, P., Kun, R., Martín-Luengo, M.A., Letaïef, S., Dékány, I. and Ruiz-Hitzky, E. (2008) Titania-Sepiolite Nanocomposites Prepared by a Surfactant Templating Colloidal Route. *Chemistry of Materials*, **20**, 84-91. <https://doi.org/10.1021/cm702251f>

- [22] Rhouta, B., Kaddami, H., Elbarqy, J., Amjoud, M., Daoudi, L., Maury, F., Senocq, F., Maazouz, A. and Gerard, J.-F. (2008) Elucidating the Crystal-Chemistry of Jbel Rhas-soul Stevensite (Morocco) by Advanced Analytical Techniques. *Clay Minerals*, **43**, 393-403. <https://doi.org/10.1180/claymin.2008.043.3.05>
- [23] Bouna, L., Rhouta, B., Amjoud, M., Jada, A., Maury, F., Daoudi, L. and Senocq, F. (2010) Correlation between Electrokinetic Mobility and Ionic Dyes Adsorption of Moroccan Stevensite. *Applied Clay Science*, **48**, 527-530. <https://doi.org/10.1016/j.clay.2010.02.004>
- [24] Lakbita, O., Rhouta, B., Maury, F., Senocq, F., Amjoud, M. and Jada, A. (2016) Supported Photocatalyst Based on CuO-TiO₂/Palygorskite Nanocomposite Material for Wastewater Treatment. *Journal of Colloid Science and Biotechnology*, **5**, 199-205. <https://doi.org/10.1166/jcsb.2016.1150>
- [25] Lakbita, O., Rhouta, B., Maury, F., Senocq, F., Amjoud, M. and Daoudi, L. (2019) On the Key Role of the Surface of Palygorskite Nanofibers in the Stabilization of Hexagonal Metastable β -Ag₂CO₃ Phase in Palygorskite-Based Nanocomposites. *Applied Clay Science*, **172**, 123-134. <https://doi.org/10.1016/j.clay.2019.02.023>
- [26] Rhouta, B., Bouna, L., Maury, F., Senocq, F., Lafont, M.C., Jada, A., Amjoud, M. and Daoudi, L. (2015) Surfactant-Modifications of Na⁺-Beidellite for the Preparation of TiO₂-Bd Supported Photocatalysts: II-Physico-Chemical Characterization and Photocatalytic Properties. *Applied Clay Science*, **115**, 266-274. <https://doi.org/10.1016/j.clay.2015.04.025>
- [27] Bouna, L., Rhouta, B., Amjoud, M., Maury, F., Lafont, M.-C., Jada, A., Senocq, F. and Daoudi, L. (2011) Synthesis, Characterization and Photocatalytic Activity of TiO₂ Supported Natural Palygorskite Microfibers. *Applied Clay Science*, **52**, 301-311. <https://doi.org/10.1016/j.clay.2011.03.009>
- [28] Rhouta, B., Zatile, E., Bouna, L., Lakbita, O., Maury, F., Daoudi, L., Lafont, M.C., Amjoud, M., Senocq, F., Jada, A. and Ait Aghzzaf, A. (2013) Comprehensive Physicochemical Study of Dioctahedral Palygorskite-Rich Clay from Marrakech High Atlas (Morocco). *Physics and Chemistry of Minerals*, **40**, 411-424. <https://doi.org/10.1007/s00269-013-0579-3>
- [29] Bouna, L., Rhouta, B., Daoudi, L., Maury, F., Amjoud, M., Senocq, F., Lafont, M.C., Jada, A. and Aghzzaf, A. (2012) Mineralogical and Physico-Chemical Characterizations of Ferruginous Beidellite-Rich Clay from Agadir Basin (Morocco). *Clays and Clay Minerals*, **60**, 278-290. <https://doi.org/10.1346/CCMN.2012.0600305>
- [30] Bouna, L., Rhouta, B., Maury, F., Jada, A., Senocq, F. and Lafont, M.-C. (2014) Photocatalytic Activity of TiO₂/Stevensite Nanocomposites for the Removal of Orange G from Aqueous Solutions. *Clay Minerals*, **49**, 417-428. <https://doi.org/10.1180/claymin.2014.049.3.05>
- [31] Hofstadler, K., Bauer, R., Novalic, S. and Heisler, G. (1994) New Reactor Design for Photocatalytic Wastewater Treatment with TiO₂ Immobilized on Fused-Silica Glass Fibers: Photomineralization of 4-Chlorophenol. *Environmental Science & Technology*, **28**, 670-674. <https://doi.org/10.1021/es00053a021>
- [32] Sarantopoulos, C., Puzenat, E., Guillard, C., Herrmann, J.-M., Gleizes, A.N. and Maury, F. (2009) Microfibrous TiO₂ Supported Photocatalysts Prepared by Metal-Organic Chemical Vapor Infiltration for Indoor Air and Waste Water Purification. *Applied Catalysis B: Environmental*, **91**, 225-233. <https://doi.org/10.1016/j.apcatb.2009.05.029>
- [33] Lakbita, O., Rhouta, B., Maury, F., Senocq, F., Amjoud, M. and Daoudi, L. (2019) Influence of the Crystal Structure of Ag₂CO₃ on the Photocatalytic Activity under

- Visible Light of Ag₂CO₃-Palygorskite Nanocomposite Material. *Applied Surface Science*, **464**, 205-211. <https://doi.org/10.1016/j.apsusc.2018.09.053>
- [34] Bouna, L., Rhouta, B. and Maury, F. (2013) Physicochemical Study of Photocatalytic Activity of TiO₂ Supported Palygorskite. *International Journal of Photoenergy*, **2013**, 2-7. <https://doi.org/10.1155/2013/815473>
- [35] Correia, F., Goetz, V., Plantard, G. and Sacco, D. (2011) A Model for Solar Photocatalytic Mineralization. *Journal of Solar Energy Engineering, Transactions of the ASME*, **133**, 2-6. <https://doi.org/10.1115/1.4004242>
- [36] Plantard, G., Janin, T., Goetz, V. and Brosillon, S. (2012) Solar Photocatalysis Treatment of Phytosanitary Refuses: Efficiency of Industrial Photocatalysts. *Applied Catalysis B: Environmental*, **115-116**, 38-44. <https://doi.org/10.1016/j.apcatb.2011.11.034>
- [37] Plantard, G. and Goetz, V. (2014) Correlations between Optical, Specific Surface and Photocatalytic Properties of Media Integrated in a Photo-Reactor. *Chemical Engineering Journal*, **252**, 194-201. <https://doi.org/10.1016/j.cej.2014.04.055>
- [38] Janin, T., Goetz, V., Brosillon, S. and Plantard, G. (2013) Solar Photocatalytic Mineralization of 2,4-Dichlorophenol and Mixtures of Pesticides: Kinetic Model of Mineralization. *Solar Energy*, **87**, 127-135. <https://doi.org/10.1016/j.solener.2012.10.017>
- [39] Sun, Z.-G., Li, X.-S., Zhu, X., Deng, X.-Q., Chang, D.-L. and Zhu, A.-M. (2014) Facile and Fast Deposition of Amorphous TiO₂ Film under Atmospheric Pressure and at Room Temperature, and Its High Photocatalytic Activity under UV-C Light. *Chemical Vapor Deposition*, **20**, 8-13. <https://doi.org/10.1002/cvde.201307088>
- [40] Plantard, G., Goetz, V. and Sacco, D. (2011) TiO₂-Coated Foams as a Medium for Solar Catalysis. *Materials Research Bulletin*, **46**, 231-234. <https://doi.org/10.1016/j.materresbull.2010.11.011>
- [41] Herrmann, J.M. (2010) Photocatalysis Fundamentals Revisited to Avoid Several Misconceptions. *Applied Catalysis B: Environmental*, **99**, 461-468. <https://doi.org/10.1016/j.apcatb.2010.05.012>
- [42] Malato, S., Blanco, J., Vidal, A. and Richter, C. (2002) Photocatalysis with Solar Energy at a Pilot-Plant Scale: An Overview. *Applied Catalysis B: Environmental*, **37**, 1-15. [https://doi.org/10.1016/S0926-3373\(01\)00315-0](https://doi.org/10.1016/S0926-3373(01)00315-0)